Fuel 177 (2016) 87–106

Contents lists available at ScienceDirect

Fuel

journal homepage: www.elsevier.com/locate/fuel

Comparison of evaporation rate and heat flow models for prediction of Liquefied Natural Gas (LNG) ageing during ship transportation

Mario Miana *, Rafael del Hoyo, Vega Rodrigálvarez

ITAINNOVA – Instituto Tecnológico de Aragón, Operations Unit, María de Luna 7 – 8, 50018 Zaragoza, Spain

HIGHLIGHTS

- Two LNG ageing models are compared with published results and 558 real LNG voyages.
- The 1st model is based on a constant or variable evaporation rate over time.
- The 2nd model is based on a heat flow computed at the start or the end of the voyage.
- Evaporation rate models are more accurate to overcome LNG ageing uncertainties.
- In addition, the influences of ship capacity and voyage duration are described.

ARTICLE INFO

Article history:
Received 14 October 2015
Received in revised form 20 November 2015
Accepted 23 February 2016
Available online 3 March 2016

Keywords:
Liquefied Natural Gas ageing
Weathering
Boil-off rate
LNG carrier
Constant heat flow
Evaporation rate

ABSTRACT

The prediction of ageing phenomena in Liquefied Natural Gas is based on two hypotheses: considering evaporation rate or considering heat flow transferred to the hydrocarbons mixture. This paper proposes two models based on these premises and validates them against other numerical models described in the scientific literature. Then, the results of the two ageing approaches are compared with a database containing experimental measurements at the loading and unloading ports for 558 voyages by a number of different LNG carriers. The weathering models based on evaporation rate are more accurate than ageing models based on heat flow for the following variables at the discharge port: Methane content, Higher Heating Value, Wobbe Index, Liquid Density, LNG volume and temperature. The effects of ship capacity and voyage duration on accuracy are also described. Finally, the evolution over time of the aforementioned variables is reported for a specific voyage.

1. Introduction

In 2014, Natural Gas accounted for 25% of global energy consumption and Liquefied Natural Gas (LNG) met 10% of the global demand for Natural Gas. A measurable consequence of the growth in the LNG trade is the expansion of the LNG fleet. This fleet was composed by 373 ships at the end of 2014, 28 of them were delivered in 2014 [1]. This expansion is expected to go on the future: the forecast up to 2035 predicts a demand growth of 1.9% per year [2]. One of the main concerns in LNG ship transportation is ageing or weathering. This phenomenon is the change in LNG composition over time because LNG is shipped close to its boiling point and, if a certain heat flow is received from the sea water or from elsewhere, it causes the inhomogeneous evaporation of the LNG mixture into Boil-Off Gas (BOG). This is the result of the different boiling temperatures of LNG components and leads to a significant evaporation of lighter components, mainly Nitrogen (N2) and Methane (C1). The changes in C1 and N2 contents in LNG significantly alter properties such as the Wobbe Index, Higher Heating Value and Liquid Density [3].

The scientific literature concerning LNG ageing started with the pioneer report from Acker and Moulton [4], who measured the evolution in time of LNG composition, temperature and mass contained in a vehicle size tank under constant heat flow transferred to the mixture and proposed a flash boiling model to predict this phenomenon. Next, Shah and Arts [5] developed a specific ageing model for LNG storage tanks based on mass and energy balances and applied it to simulate the weathering in a typical flat bottom, above-ground LNG tank and during the cargo voyage of an LNG ship of 125,000 m^3. In the same manner, the experimental and numerical works of Kountz [6] described the weathering phenomena under constant heat flow in pressurized vehicle size tanks for LNG mixtures having N2 content up to 6%. Aspelund et al. [7] developed a physical model to predict the LNG ageing phenomena under constant heat flow in small LNG-chains. Both models were

* Corresponding author. Tel.: +34 976 01 11 57; fax: +34 976 01 18 89.
E-mail address: mmiana@itainnova.es (M. Miana).

http://dx.doi.org/10.1016/j.fuel.2016.02.070
0016-2361/

Nomenclature

E	energy (kJ)
e	error, defined in Eq. (31), dimensionless
F	vapour fraction, dimensionless
H	enthalpy (kJ/kmol)
K	equilibrium constant, dimensionless
n	molar quantity (kmol)
$\dot{n}$	molar flow rate (kmol/s)
P	pressure (Pa)
Q	heat flow (kW)
T	temperature (°C)
t	time (s)
U	internal energy (kJ/kmol)
V	volume (m^3)
X	molar composition of liquid phase, dimensionless
Y	molar composition of vapour phase, dimensionless
Z	molar composition of LNG mixture, dimensionless
$\%_L$	percentage of the ship capacity filled by LNG, dimensionless

Greek symbols

ε	difference, defined in Eq. (28), dimensionless
ϕ	variable to be compared
ρ	molar density (kmol/m^3)
Δ	change

Subscripts

Dsc	variable measured at the discharge port
Eq	variable calculated at thermodynamic equilibrium
Ev	evaporated
Exp	variable stored in the experimental database
i	ageing model
Iter, *m*	iteration
L	liquid
Ld	variable measured at loading port
Out	vented gas flow taken out of the tank to avoid significant changes in pressure
Ref	data published in reference paper
Ship	full ship
V	vapour
Voyage	total voyage duration

Superscripts

t	calculated variable at the current time step
$t + \Delta t$	calculated variable at the following time step
*	estimated variable from molar balances

Acronyms

BOG	Boil-Off Gas
BOR	Boil-Off Rate, defined in Eq. (14) (percentage of evaporated mols with respect to the initial liquid mols per day)
C1	Methane
C2	Ethane
C3	Propane
GERG2004	equation of state for LNG and Natural Gas developed by the European Gas Research Group in 2004
HHV	Higher Heating Value (MJ/m^3);
HNGC	Handy Natural Gas Carrier ($60{,}000 < V \leqslant 125{,}000$ m^3)
iC4	Isobutane
iC5	Isopentane
LD	Liquid Density (kmol/m^3)
LEE	Lee–Erbar–Edmister equation of state
LNG	Liquefied Natural Gas
LNGC	Large Natural Gas Carrier ($150{,}000 < V \leqslant 177{,}000$ m^3);
MNGC	Medium Natural Gas Carrier ($125{,}000 < V \leqslant 150{,}000$ m^3)
N2	Nitrogen
*n*C4	*n*-Butane
*n*C5	*n*-Pentane
*n*C6	*n*-Hexane
SNGC	Small Natural Gas Carrier ($V \leqslant 60{,}000$ m^3)
WI	Wobbe Index (MJ/m^3)
VLNGC	Very Large Natural Gas Carrier ($V > 177{,}000$ m^3)

based on equilibrium between liquid and vapour phases, yielding a good approximation of experimental data measured in [6]. Other related references are the vaporisation studies by Boe [8] and Conrado and Vesovic [9] concerning LNG on water, the investigation of the rollover phenomenon in storage tanks by Bates and Morrison [10] or the analysis of changes of pressure and temperature of LNG tanks by Chen et al. [11].

In recent years, Dimopoulos and Frangopoulos [12], Pellegrini et al. [13] and Migliore et al. [14] have developed specific LNG ageing models based on the constant heat flow rate to determine the evolution over time of the LNG composition when stored in tanks. In the same field, Miana et al. [15] developed a similar model, focused on LNG ageing during ship transportation, but based on a constant evaporation rate approach.

The main objective of this paper is the comparison of the heat flow and evaporation rate approaches for modelling LNG weathering during ship transportation. The problem underlying LNG ageing during ship transportation can be defined as a vented tank under constant heat flow, assuming that the temperatures of the LNG and the environment (sea water and air) are nearly constant throughout the voyage and the transferred heat flow depends only on the convective thermal resistances between the LNG and the tank wall and between the ship and the environment, together with the conductive thermal resistances through the tank walls. Based purely on this initial description, the evaporation rate approach should be discarded. However, there are specific issues regarding LNG transportation that should be considered before rejecting the evaporation rate approach outright.

Let us consider the situation of an LNG freighter arriving at a reliquefaction plant. It is important to predict the composition, the temperature, the density and the volume of the receiving LNG prior to unloading, in order to determine the best operational orders to avoid roll-over phenomena or to greatly reduce the expensive blending operations to achieve the required quality of Natural Gas to be distributed. However, the information available at the reliquefaction plant is limited: based on the information contained in the Certificate On Loading, operators may know the initial composition, the temperature and the loaded volume of LNG, the name of the ship and the departure time; this information must be enough to predict how much LNG has evaporated during ship transportation and the resulting LNG quality and the temperature prior to unloading. Nonetheless, the prediction of the amount of the Boil-Off Gas generated during ship transportation is not straightforward, as it depends on the following parameters [16]:

- the heat transfer from the sea/air environment to the LNG resulting from the temperature difference;
- the sloshing of cargo in partially filled tanks due to thermal heating caused by wave generated friction;

– the cooling of the ship's tanks during ballast voyages or before LNG loading;
– the use of LNG as fuel to power the ship.

Accurate calculations of the input heat flow based only on the insulation characteristics of the shipping containers [17–21] should take into account the thickness of the insulation barriers, variation in effective thermal conductivity depending on the temperature for the materials comprising the insulation barriers, sea water and air temperatures during the voyage and lastly, ship velocity and sailing conditions. Moreover, polyurethane foams are commonly used as insulation materials in LNG ship tanks and these materials present some ageing effects [22,23], so the conductive thermal resistance can vary over the time the ship is in service. It is important to note that specific ship descriptions, including materials used or thickness of insulation barriers are not available for commercial reasons, so it is difficult to obtain accurate heat transfer calculations [21]. The use of generalized curves [24] could allow an accurate evaluation of the total heat flow input received by LNG during ship transportation, but the curves available were obtained for ground tanks.

During LNG ship loading, additional BOG is produced by the initial chilling of the ship tanks, the vapour displacement in the ship tanks, the heat leakage through piping and vessels and the energy input from loading pumps [25]. Thus, this initial BOG should be considered in LNG ageing during ship transportation, but it cannot be determined based on the information from the Certificates On Loading. Furthermore, the typical loading operations are based on a heel, a ballast LNG loading that keeps the LNG tanks at cryogenic temperature. As a consequence, the total composition of LNG at the loading port should be corrected by the size of this heel, resulting, naturally in a different initial composition. However, the composition measured in the Certificate On Loading does not take into account these differences in composition.

Lastly, some LNG carriers have the option of using the BOG as fuel [16] given the simplicity of burning BOG in boilers to power the steam turbines. These ships can force the generation of BOG by reducing tank pressure, and this can represent another source of uncertainty when modelling LNG ageing during ship transportation. However, in recent years, new tankers have been built using other propulsion systems, including dual fuel-diesel and diesel-electric [26], but when the fuel oil price is so high, the burning of BOG is an attractive option to reduce the cost of some voyages.

Therefore, the modelling of LNG weathering during ship transportation has many uncertainties, and the laboratory models based on simple descriptions of heat transfer to a vented tank cannot accurately capture the whole LNG ageing problem during ship transportation. This paper proposes two different modelling approaches based on predefined heat flow or evaporation rates and compares the results obtained with an experimental database that has been collating the information on the LNG arriving at certain reliquefaction plants in recent years.

The present paper is organized into four sections. The first presents the main LNG weathering problems during ship transportation. The two different modelling approaches are described in Section 2. Four different models are defined in this section, characterised by constant or variable evaporation rates and heat flows calculated under the loading or discharging conditions. These models are validated in Section 2 against other numerical ageing results. Section 3 evaluates the accuracy of each weathering model, while also analysing the influence of ship capacity and voyage duration on the accuracy of the proposed models. Lastly, Section 4 summarizes the main conclusions and proposes future work to achieve a better understanding of LNG ageing phenomena during ship transportation.

2. LNG ageing modelling approaches

2.1. Definition of the problem

As stated in Section 1, the LNG ageing during ship transportation can be defined as a tank filled with a boiling liquid mixture that receives a certain amount of heat. The input heat flow causes the evaporation of the lighter components, N2 and C1 mainly. To avoid dangerous rises in pressure, some vapour mols are vented from the tank.

The loading conditions are defined by a given initial LNG composition, temperature and pressure. From this starting point, the molar and energy balances that describe the physics of this system are shown in Eqs. (1) and (2):

$$\frac{dn_{Ship}}{dt} = -\dot{n}_{Out} \tag{1}$$

$$\frac{dE_{Ship}}{dt} = Q - \dot{n}_{Out} \cdot H_{Out} \tag{2}$$

where n_{Ship} and E_{Ship} are the total LNG mols and energy stored inside the ship, $\dot{n}_{Out}$ the molar flow of vapour phase vented out of the tank having an enthalpy H_{Out} and Q the heat flow received by the LNG stored inside the containers. The molar quantity and the energy stored in the ship are divided between the liquid and vapour phases. The total energy stored in the ship at time t is computed from the internal energy of the liquid and vapour phases:

$$E^t_{Ship} = n^t_L \cdot U^t_L + n^t_V \cdot U^t_V \tag{3}$$

For the liquid phase, the molar balance is expressed in Eq. (4), considering no new liquid to be added into the system; this means that no reliquefaction systems are considered in this analysis. For the vapour phase, the molar balance must take into account the incoming flow of evaporated liquid and the venting flow rate:

$$\frac{dn_L}{dt} = -\dot{n}_{Ev} \tag{4}$$

$$\frac{dn_V}{dt} = \dot{n}_{Ev} - \dot{n}_{Out} \tag{5}$$

If the volume of the ship and the loading conditions (LNG temperature and composition) are known, the previous equations can be discretized using a first order scheme in the following way:

$$\frac{dn_L}{dt} \approx \frac{n^{t+\Delta t}_L - n^t_L}{\Delta t} = -\dot{n}^t_{Ev} \tag{6}$$

$$\frac{dn_V}{dt} \approx \frac{n^{t+\Delta t}_V - n^t_V}{\Delta t} = \dot{n}^t_{Ev} - \dot{n}^t_{Out} \tag{7}$$

$$\frac{dE}{dt} \approx \frac{E^{t+\Delta t} - E^t}{\Delta t} = Q^t - \dot{n}^t_{Out} \cdot H^t_{Out} \tag{8}$$

Following [15], the time step size is fixed to a constant value of 1800 s (0.5 h). The first assumed simplification is that at time t, the liquid and vapour phases are in thermodynamic equilibrium, in line with the Raoult law:

$$Y^t = K^t \cdot X^t \tag{9}$$

The second assumed simplification is that the tank pressure is known at all times. Since the experimental database contains only the tank pressure at the loading and unloading ports, it is assumed that there is a linear variation in pressure over time between these two values. The evolution of pressure over the course of the voyage is never available and the reported values in the literature cover vehicle size tanks [4,6].

A third assumption is performed regarding ship capacity. It is assumed that all LNG is stored in a single tank. Thus, the number of tanks, their volumes and their shape are not considered in this study.

The LNG stored in the ship is a mixture of liquid and vapour phases having a composition Z^t. The specific compositions of liquid and vapour phases are related to the composition of the mixture by means of the vapour fraction F^t:

$$Z^t = (1 - F^t) \cdot X^t + F^t \cdot Y^t \tag{10}$$

Thus, the state at time t is known if LNG composition, temperature and pressure are defined. The equilibrium constants, vapour fraction, internal energy, enthalpy and density of liquid and vapour phases are then calculated at the saturation state by means of the Lee–Erbar–Edmister state equations [27,28], the Rijkers and Heidemann solution method [29] and the McCarty model [30]. These calculations are performed using the thermodynamic functions described in Table 1. The number of liquid and vapour mols can be calculated if the total ship volume and the percentage of the volume occupied by the liquid phase are known:

$$V_{Ship} = \frac{n_L^t}{\rho_L^t} + \frac{n_V^t}{\rho_V^t} \tag{11}$$

$$V_L^t = \frac{n_L^t}{\rho_L^t} = V_{Ship} \cdot \%_L^t \tag{12}$$

In summary, all thermodynamic properties and the number of mols in both liquid and vapour phases are available at the beginning of each time step and pressure is also available at the end of each time step. The calculation of the next equilibrium state for the following time step requires an estimation of the LNG composition and temperature in order to find the thermodynamic properties (internal energy, density and enthalpy) and to solve the molar and the energy balance described above. As a conclusion, the unknown variables are:

- for the current time: evaporated and vented mol flows ($\dot{n}_{Ev}^t, \dot{n}_{Out}^t$) and heat flow received by the LNG mixture (Q^t).
- for the following time: LNG temperature and composition and percentage of volume occupied by the liquid phase ($\%_L^t$).

Table 1
Thermodynamic functions.

Function name	Input data	Output data	Comment
ETLV	Z, P	T_{Eq}	Provides the equilibrium temperature for a liquid–vapour LNG mixture at a given pressure
FL	Z, P, T_{Eq}	K, F	Provides the equilibrium constants and the vapour fraction of a LNG mixture for a given composition, operating pressure and equilibrium temperature
LDF	X, P, T_{Eq}	ρ_L	Provides Liquid Density of a LNG liquid phase for a given operating pressure and equilibrium temperature
HV	Y, P, T_{Eq}	H_L	Provides vapour enthalpy of a LNG vapour phase for a given operating pressure and equilibrium temperature
UL	X, P, T_{Eq}	U_L	Provides liquid internal energy of a LNG liquid phase for a given operating pressure and equilibrium temperature
UV	Y, P, T_{Eq}	U_V	Provides vapour internal energy of a LNG vapour phase for a given operating pressure and equilibrium temperature
VDF	Y, P, T_{Eq}	ρ_V	Provides vapour density of a LNG vapour phase for a given operating pressure and equilibrium temperature
XY	Z, F, K_i	X, Y	Provides the composition of liquid and vapour phases from the composition, the vapour fraction and the equilibrium constants of a LNG mixture

The solution to the molar and the energy balances in Eqs. (6)–(8) requires the calculation of the flow of evaporated mols or the input heat flow and an iterative procedure to obtain the temperature for the following time. These procedures are explained in Sections 2.2 and 2.3.

2.2. Modelling ageing by evaporation rate

The model considering the evaporation rate is a simplification of one previously presented by Miana et al. [15], hence only a brief description is given here. Fig. 1a describes the flow chart for this ageing model, composed by an initial block and temporal block. The initial block calculates the initial equilibrium state from the loading data. The assumption of the thermodynamic equilibrium is imposed from the beginning of the voyage, so the loading temperature is not used for the evaporation rate ageing model and the initial equilibrium temperature is directly calculated by the *ETLV* function. Then, the equilibrium constants K and the vapour fraction F are obtained using the *FL* function. These results are further applied to calculate the equilibrium composition of the liquid (X) and vapour (Y) phases before the liquid and vapour densities are estimated by *LDF* and *VDF* functions. The loaded volume defined in the Certificate On Loading is assumed to be the initial liquid volume stored in the ship, hence the vapour volume is the net capacity of the ship minus this initial liquid volume. Once the volumes and densities of liquid and vapour phases are obtained, the initial number of liquid and vapour mols can be estimated.

At this point, the temporal loop starts. A count variable called m is initialized to 0 at the beginning of each time step and the pressure at the following time step is calculated using Eq. (13):

$$P^{t+\Delta t} = P^t + \frac{P_{Dsc} - P_{Ld}}{t_{voyage}} \Delta t = P^t + \Delta P \tag{13}$$

The key parameter in this approach is BOR, which is defined as the percentage of the LNG mols vaporised over the whole voyage with respect to the LNG mols loaded at the port of origin divided by the total voyage duration:

$$\mathrm{BOR} = \frac{n_{Ev}}{n_{Ld} \cdot t_{voyage}} \cdot 100 \tag{14}$$

A common approach is to express BOR in terms of the initial loaded volume and the discharge volume if variations in LNG density are reduced during ship transportation. This simplification is quite useful for reliquefaction operators because they can easily access loaded and unloaded LNG volumes rather than LNG mols. In concordance with this, the experimental database contains only the loading and unloading LNG volumes, together with the duration of the voyage, hence the BOR is estimated as:

$$\mathrm{BOR} = \frac{V_{Ld} - V_{Dsc}}{V_{Ld}} \frac{24 \cdot 3600}{t_{voyage}} \cdot 100 \tag{15}$$

As the molar densities of LNG are assumed to be constant during ship transportation, the evaporated mols during a certain time step Δt can be easily calculated from BOR and the time step size:

$$n_{Ev}^t = \dot{n}_{Ev}^t \cdot \Delta t = \frac{\mathrm{BOR} \cdot n_{Ld}}{24 \cdot 3600 \cdot 100} \cdot \Delta t \tag{16}$$

One of the main advantages of using BOR is that reported values can be found elsewhere: values of 0.10–0.15% are common for fully laden voyages and 0.06–0.10% for ballast voyages [16]. Moreover, as these values are based on experimental results, they include all the uncertainties noted in Section 1.

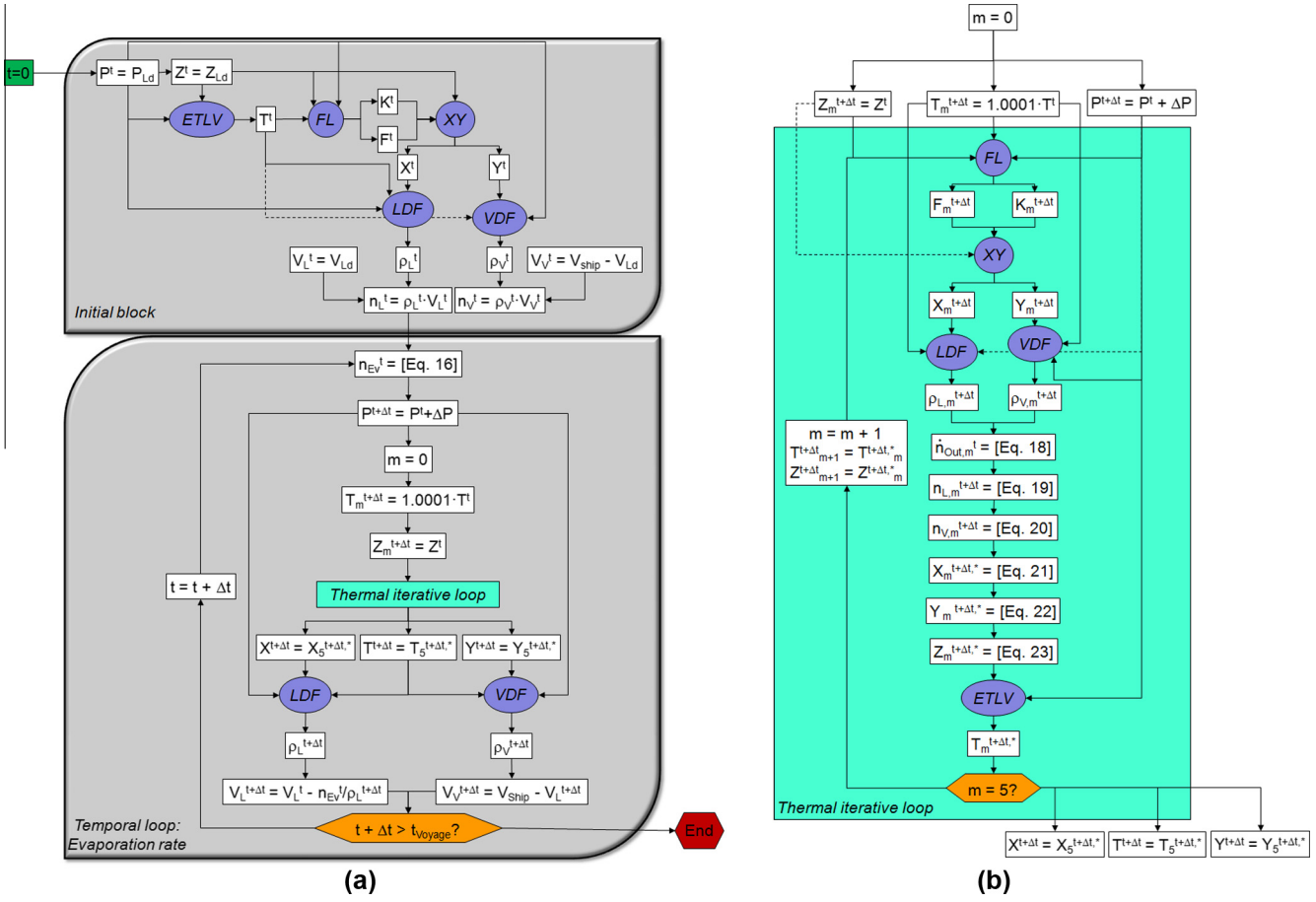

Fig. 1. Flow charts for ageing models based on evaporation rate: general description (a) and thermal iterative loop to obtain the temperature at the following time step (b).

Once the flow of evaporated mols is known, the flow of vented mols can be calculated directly using Eq. (18), considering that the total volume of the ship is fully occupied by the liquid and vapour phase at time t and at time $t + \Delta t$ according to Eq. (17):

$$V_{Ship} = \frac{n_L^t}{\rho_L^t} + \frac{n_V^t}{\rho_V^t} = \frac{n_L^{t+\Delta t}}{\rho_L^{t+\Delta t}} + \frac{n_V^{t+\Delta t}}{\rho_V^{t+\Delta t}}. \tag{17}$$

$$\dot{n}_{Out,m}^t = \frac{n_V^t}{\Delta t} - \frac{\rho_{V,m}^{t+\Delta t} \cdot V_{Ship}}{\Delta t} + \frac{\rho_{V,m}^{t+\Delta t}}{\rho_{L,m}^{t+\Delta t}} \frac{n_L^t}{\Delta t} + \left(1 - \frac{\rho_{V,m}^{t+\Delta t}}{\rho_{L,m}^{t+\Delta t}}\right) \dot{n}_{Ev}^t \tag{18}$$

However, the solution to Eq. (18) requires the densities of the liquid and vapour phases at the following time step. A simple thermal iterative method is employed to accomplish this. The method is depicted in Fig. 1b. For the initial iteration ($m = 0$), the temperature at the following time step is initially supposed to be 0.01% larger than the temperature at the current time step. Likewise, the LNG mixture composition at the following time step is assumed to be equal to the composition at the current time step. The supposed values for temperature and composition at the following time step allow the equilibrium constants, the liquid and vapour compositions and the liquid and vapour densities to be estimated for the following time step. Once Eq. (18) is solved, the molar balances of Eqs. (19) and (20) yield the liquid and vapour moles present at the end of the time step:

$$n_{L,m}^{t+\Delta t} = n_L^t - \dot{n}_{Ev}^t \cdot \Delta t \tag{19}$$

$$n_{V,m}^{t+\Delta t} = n_V^t + n_{Ev}^t - (\dot{n}_{Out,m}^t \cdot \Delta t) \tag{20}$$

These data are then applied to a molar balance for the liquid phase to obtain Eq. (21) as an estimated approach for the liquid composition at the following time step:

$$X_m^{t+\Delta t,*} = X^t \frac{n_L^t + n_V^t \cdot K_m^t}{K_m^{t+\Delta t}\left(n_{V,m}^{t+\Delta t} + \dot{n}_{Out,m}^{t+\Delta t} \cdot \Delta t\right) + n_L^{t+\Delta t}} \tag{21}$$

where estimated variables from molar balances are denoted by superscript (*).

The estimated liquid composition is now used to obtain vapour and mixture compositions from the previously calculated vapour fraction and equilibrium constants, under Eqs. (22) and (23):

$$Y_m^{t+\Delta t,*} = X_m^{t+\Delta t,*} \cdot K_m^{t+\Delta t,*} \tag{22}$$

$$Z_m^{t+\Delta t,*} = \left(1 - F_m^{t+\Delta t}\right) \cdot X_m^{t+\Delta t,*} + F_m^{t+\Delta t} \cdot Y_m^{t+\Delta t,*} \tag{23}$$

The *ETLV* function computes the next estimated equilibrium temperature ($T_m^{t+\Delta t,*}$) from the estimated mixture composition ($Z_m^{t+\Delta t,*}$) and operating pressure ($P^{t+\Delta t}$). The iterative loop is repeated 5 times, starting from the estimated equilibrium temperature ($T_m^{t+\Delta t,*}$) and the mixture composition ($Z_m^{t+\Delta t,*}$). After these 5 iterations, the values obtained for the temperature, LNG mixture composition and volumes occupied by liquid and vapour phases are updated and the iterative loop is repeated at the following time step through to the end of the voyage.

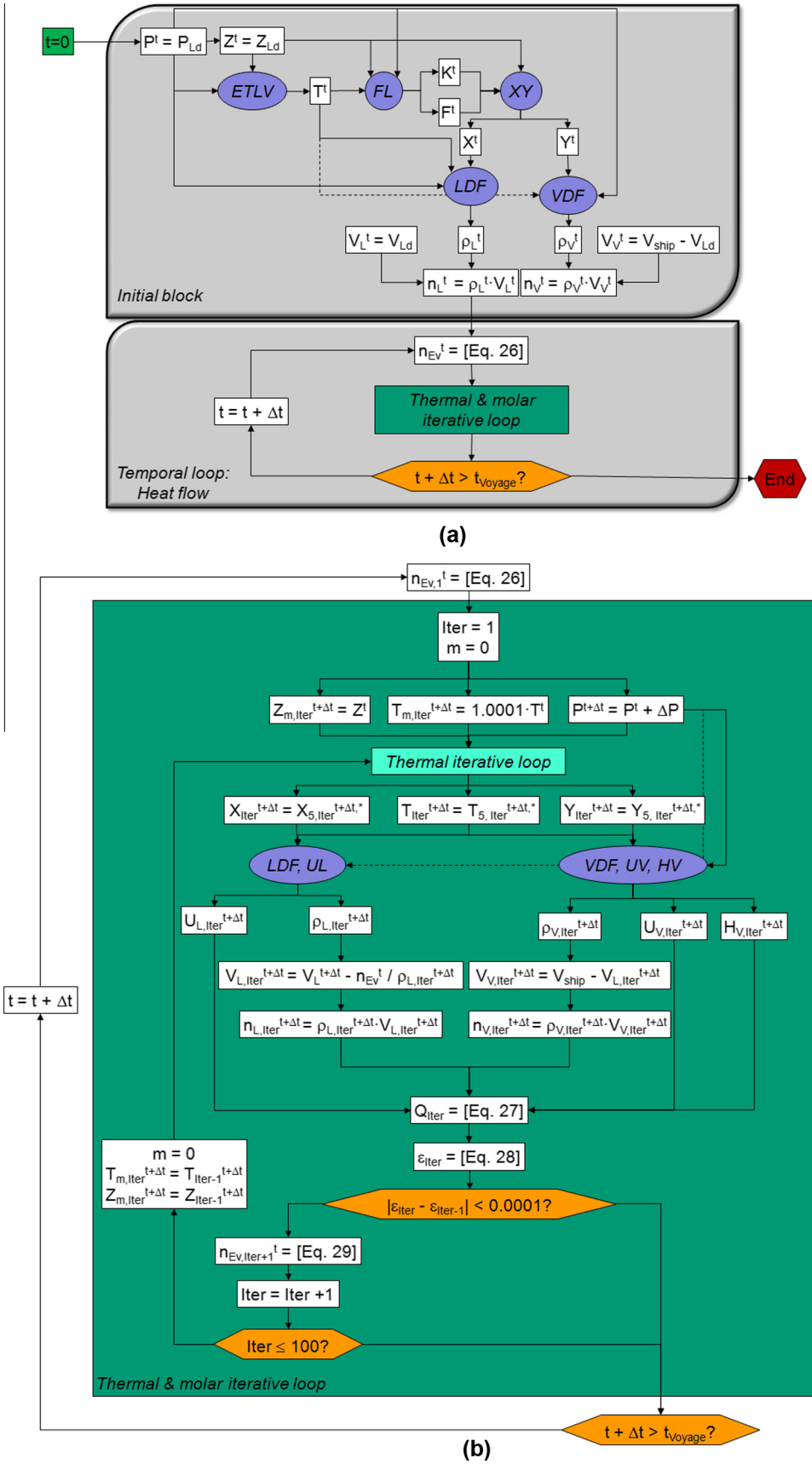

Fig. 2. Flow charts for ageing models based on heat flow: general description (a) and thermal & molar iterative loop to obtain the temperature and the number of evaporated mols at the following time step (b).

Table 2
Validation with data from Shah and Aarts [5].

Reference data								
Variable	Units	Case 1	Case 2	Case 5	Case 6	Case 7	Case 8	Case 9
V_{Ship}	m^3	47,691	47,691	47,691	47,691	47,691	47,691	125,000
BOR	%/day	0.05	0.05	0.05	0.05	0.05	0.05	0.25
Q	W	58,556	117,111	58,556	58,556	58,556	58,556	729,017
	BTU/h	$2 \cdot 10^5$	$4 \cdot 10^5$	$2 \cdot 10^5$	$2 \cdot 10^5$	$2 \cdot 10^5$	$2 \cdot 10^5$	$2.49 \cdot 10^6$
P	mbar	1034.25	1034.25	1034.25	1034.25	1034.25	1034.25	1075.62
Duration	days	270	270	280	280	280	280	12
$C1_{Ld}$	%	88.0	88.0	95.0	100.0	95	90.0	87.55
$C2_{Ld}$	%	7.0	7.0	0.0	0.0	5.0	5.0	8.14
$C3_{Ld}$	%	2.5	2.5	0.0	0.0	0.0	5.0	2.3
$iC4_{Ld}$	%	0.5	0.5	0.0	0.0	0.0	0.0	1.16
$N2_{Ld}$	%	2.0	2.0	5.0	0.0	0.0	0.0	0.85
T_{Ld}	°C	−165.51	–	–	–	–	–	−161.93
T_{Dsc}	°C	−160.92	–	–	–	–	–	−160.97
HHV_{Ld}	kJ/m^{3**}	40,778	40,778	35,810	37,673	39,018	41,916	41,983
	BTU/scf	1094	1094	961	1011	1047	1125	1127
HHV_{Dsc}	kJ/m^{3**}	41,937	42,765	37,466	37,673	39,329	42,537	42,227
	BTU/scf	1126	1148	1006	1011	1056	1141	1133
$\rho_{L,Ld}$	kmol/m^3	–	–	–	–	–	–	472.79
	lbm/ft^3	–	–	–	–	–	–	29.52
$\rho_{L,Dsc}$	kmol/m^3	–	–	–	–	–		471.12
	lbm/ft^3	–	–	–	–	–	–	29.41

Results from ageing models								
Variable	Ageing model	Case 1	Case 2	Case 5	Case 6	Case 7	Case 8	Case 9
T_{Dsc} (°C)	n_{Ev} = Const	−159.97 (0.5919%)	–	–	–	–	–	−160.70 (0.1697%)
	$n_{Ev} = f(t)$	−160.05 (0.5420%)	–	–	–	–	–	−160.72 (0.1573%)
	Q = Const	−160.68 (0.1497%)	–	–	–	–	–	−161.23 (−0.1627%)
HHV_{Dsc} (kJ/m^{3**})	n_{Ev} = Const	42,131 (−0.4631%)	42,131 (1.4818%)	37,583 (−0.3124%)	37,706 (−0.0881%)	39,369 (−0.1020%)	42,672 (−0.3166%)	42,308 (−0.2211%)
	$n_{Ev} = f(t)$	42,072 (−0.3227%)	42,072 (1.6194%)	37,553 (−0.2337%)	37,706 (−0.0881%)	39,347 (−0.0457%)	42,603 (−0.1547%)	42,303 (−0.2108%)
	Q = Const	41,817 (0.2854%)	42,370 (0.9226%)	37,177 (0.7703%)	37,706 (−0.0881%)	39,360 (−0.0791%)	42,645 (−0.2544%)	42,199 (0.0366%)
$\rho_{L,Dsc}$ (kg/m^3)	n_{Ev} = Const	–	–	–	–	–	–	466.24 (1.0335%)
	$n_{Ev} = f(t)$	–	–	–	–	–	–	466.26 (1.0287%)
	Q = Const	–	–	–	–	–	–	466.90 (0.8939%)

** Values calculated at normal conditions (0 °C and 1 bar).

2.3. Modelling ageing by heat flow

The first parameter that must be determined prior to ageing calculation is the heat flow transferred from the environment to the LNG contained in the ship tanks. As previously stated, the literature does not provide a definitive answer to this topic, given the difficulties performing a detailed thermal analysis for on board tanks. A comparison is made with scale laboratory tests, where the input heat flow is well measured [4,6,13], while it is difficult to adapt the information from other sources [17–21] to this situation due to the large number of ships in the current database.

To overcome this latter problem, the heat flow is calculated from a simple energy balance based on the available experimental data. Given the composition, temperature, pressure and volume occupied by the liquid phase at both loading and discharge ports, the exchanged heat flow can be estimated using Eq. (24):

$$Q_{Exp} = \frac{n_{L,Dsc} \cdot U_{L,Dsc} + n_{V,Dsc} \cdot U_{V,Dsc} - n_{L,Ld} \cdot U_{L,Ld} - n_{V,Ld} \cdot U_{V,Ld} + n_{Out} \cdot H_{V,??}}{t_{voyage}} \tag{24}$$

The change in composition and temperature of the LNG mixture yields two limiting approaches to estimate the enthalpy of the vented mols: at the loading port or at the discharge port. The difference between these will be shown in Section 3.

The vented mols are easily calculated from the molar balance in Eq. (25):

$$n_{Out} = n_{L,Dsc} + n_{V,Dsc} - n_{L,Ld} - n_{V,Ld} \tag{25}$$

Fig. 2a shows the flow chart when the ageing model based on heat flow is applied. As there are two main unknown variables at the end of each time step – the evaporated mols and the temperature – two iterative loops must be applied. First, an initial estimate of the evaporated mols is used and subsequently, the temperature at the end of the time step is estimated using the thermal iterative loop described in Fig. 1b. Once the thermodynamic state is fully defined for the following time step, the exchanged heat flow is calculated and compared to the experimental heat flow computed using Eq. (24). The updating of the evaporated mols to achieve the exchanged heat flow is performed by the thermal & molar iterative loop depicted in Fig. 2b.

The description of the time loop for the ageing model defined by heat flow starts with an initial estimation of the number of evaporated mols. As the BOR parameter is the best approach, it is applied for the first iteration at the beginning of each time step ($Iter = 1$) following Eq. (26):

$$n^t_{Ev,1} = \frac{BOR \cdot \Delta t}{24 \cdot 3600 \cdot 100} \cdot n_{Ld} \tag{26}$$

Table 3
Validation with data from Dimopoulos and Frangopoulos [12].

Variable	Model	C1	C2	C3	C4	N2
LNG_{Ld}	[12]	89.9	6.0	2.2	1.5	0.4
BOG_{Ld}	[12]	92.65	0.0	0.0	0.0	7.34
	LEE	88.19 (4.8191%)	0.0065 (–)	0.0 (–)	0.0 (–)	11.81–60.8774%
	GERG2004	87.92 (5.1058%)	0.0094 (–)	0.0 (–)	0.0 (–)	12.07–64.4565%
X_{Dsc}	[12]	89.70	6.24	2.29	1.56	0.22
	n_{Ev} = Const	89.8016 (−0.1133%)	6.2157 (0.3893%)	2.2792 (0.4716%)	1.5540 (0.3846%)	0.1495 (32.0659%)
	$n_{Ev} = f(t)$	89.8114 (−0.1242%)	6.2051 (0.5596%)	2.2753 (0.6421%)	1.5513 (0.5552%)	0.1569 (28.6931%)
	Q = Const	89.4955 (0.2280%)	6.4677 (−3.6496%)	2.3717 (−3.5698%)	1.6171 (−3.6604%)	0.0479 (78.2131%)
Y_{Dsc}	[12]	96.8	0.01	0.0	0.0	3.15
	n_{Ev} = Const	95.5906 (1.2494%)	0.0088 (12.4501%)	0.0 (–)	0.0 (–)	4.4006 (−39.7011%)
	$n_{Ev} = f(t)$	95.3786 (1.4683%)	0.0087 (13.0057%)	0.0 (–)	0.0 (–)	4.6126 (−46.4325%)
	Q = Const	98.5463 (−1.8040%)	0.0097 (2.7010%)	0.0 (–)	0.0 (–)	1.4439 (54.1609%)

The pressure at the following time step is calculated using Eq. (13) once more. The same initial approaches for the temperature and the LNG composition mixture in the following time step are applied, that is, the temperature is raised by 0.01% while the LNG composition remains unchanged. These approximations are the beginning of the first iterative loop to calculate the corresponding equilibrium temperature in the following time step. This iterative loop is identical to the one described in the previous section so it is not described again. Once the equilibrium temperature is achieved, the internal energy and the enthalpy at the following time step can be calculated, so the corresponding heat flow can be estimated using Eq. (27):

$$Q_{Iter} = \frac{n_{L,Iter}^{t+\Delta t} \cdot U_{L,Iter}^{t+\Delta t} + n_{V,Iter}^{t+\Delta t} \cdot U_{V,Iter}^{t+\Delta t} - n_L^t \cdot U_L^t + n_V^t \cdot U_V^t}{\Delta t} + \dot{n}_{Out,Iter}^t \cdot H_{V,Iter}^{t+\Delta t} \quad (27)$$

This estimated heat flow is compared with the experimental heat flow obtained through Eq. (24) by means of the residual defined by Eq. (28):

$$\varepsilon_{Iter} = Q_{Exp} - Q_{Iter} \quad (28)$$

This residual is compared with the residual from the previous iteration. For the first iteration, the residual of the previous iteration is set to 0 W. If the absolute value of the difference between the two residuals is less than 0.0001 W, it is assumed that the obtained solution is converged and the temporal loop moves onto the next time step. Meanwhile, the number of evaporated mols in the current time step is updated using Eq. (29):

$$n_{Ev,Iter+1}^t = n_{Ev,Iter}^t \frac{Q_{Exp}}{Q_{Iter}} \quad (29)$$

The thermal & molar iterative loop to calculate the number of evaporated mols is repeated for a maximum of 100 iterations.

2.4. Definition of the numerical models to be analysed

Four different models are built from the general evaporation rate and heat flow ageing approaches described in Sections 2.2 and 2.3. The evaporation rate is modelled from the constant evaporation rate defined in Eq. (13), and one additional model is defined by considering the variable evaporation rate defined in Eq. (30), where the liquid mols at the current time step are used to estimate the evaporated mols:

$$n_{Ev}^t = \frac{BOR \cdot \Delta t}{24 \cdot 3600 \cdot 100} \cdot n_L^t \quad (30)$$

Although BOR is still considered a constant parameter, Eq. (30) considers that the evaporated mols have decreased over time. This approach is intended to encompass the greater evaporation rate during the loading of LNG into the ship tanks. The evolution over time of BOR displayed in [12] shows a parabolic profile with a minimum at about 8 days after loading. Then, this model tries to simulate the different evaporation rates since the loading of the LNG and the larger N2 content at the beginning of the voyage can yield a significant reduction in the Boil-Off Rate.

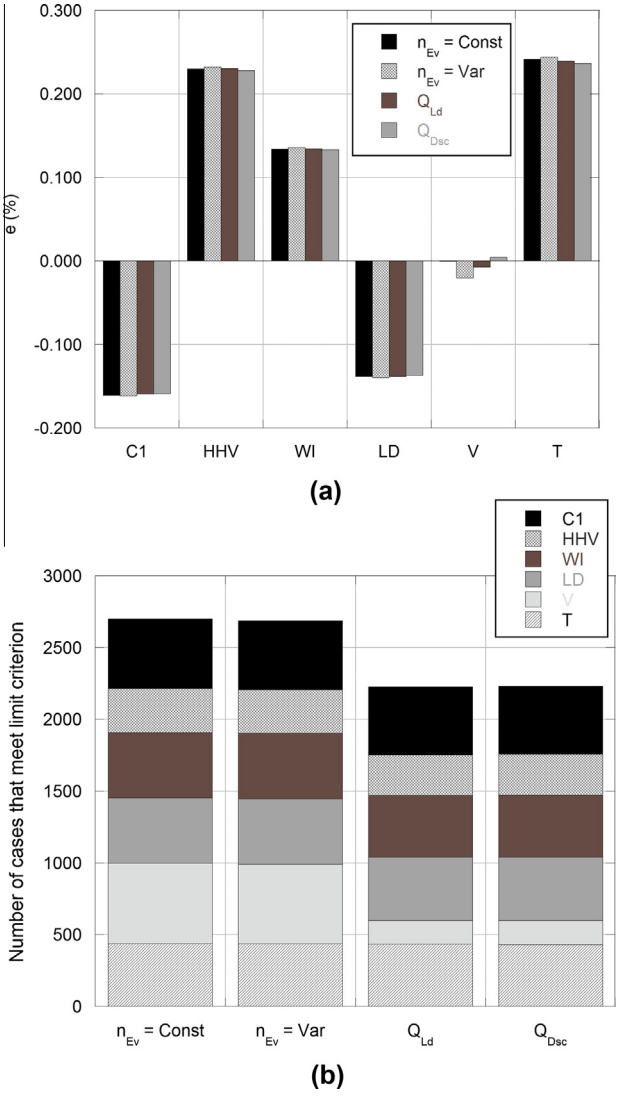

Fig. 3. Histograms of the relative differences in C1, HHV, LD, vol and temperature for the ageing models (a) and number of cases which meet the error limitation criteria (b).

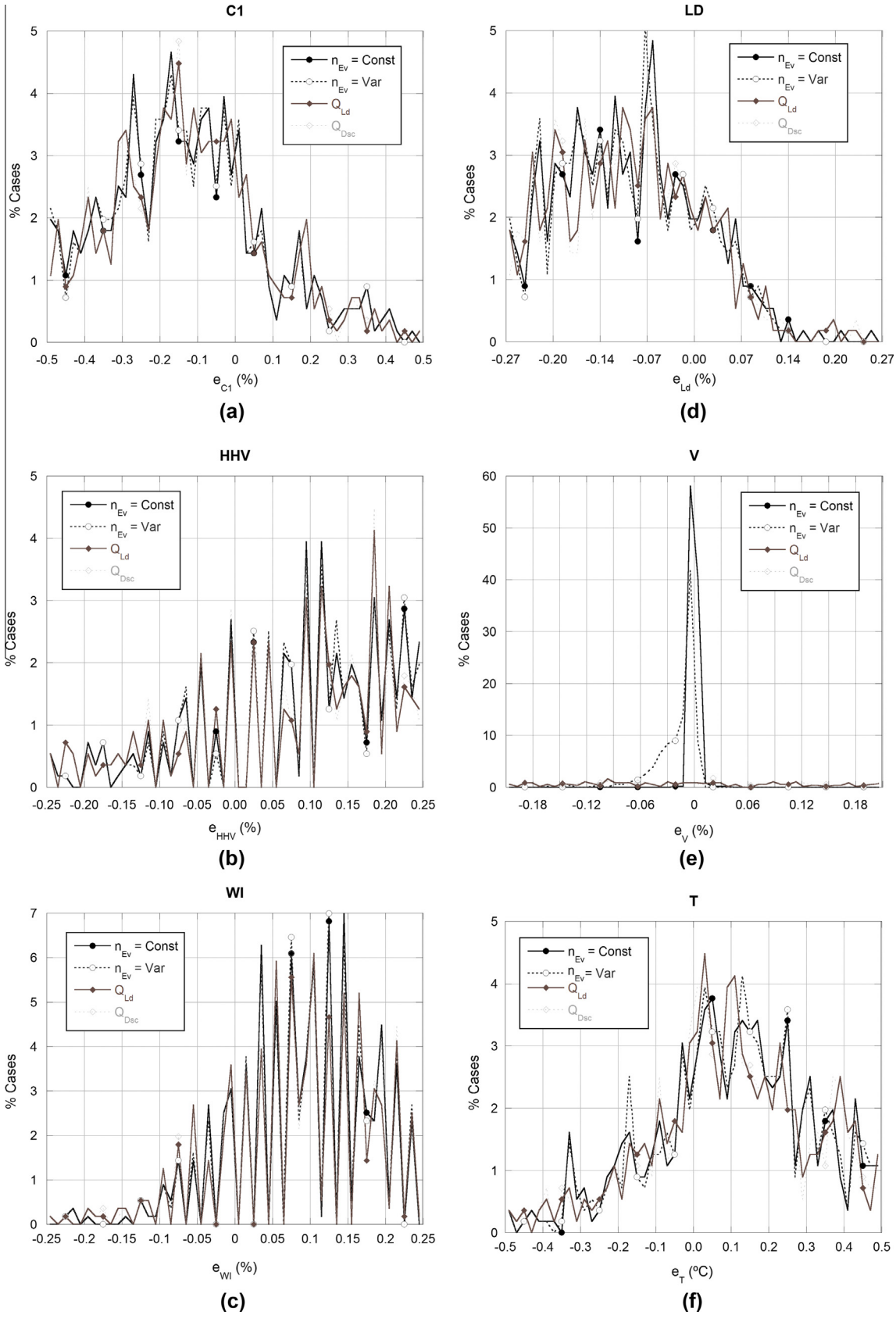

Fig. 4. Percentages of cases inside the error limits for C1 (a), HHV (b), WI (c), LD (d), volume (e) and temperature (f).

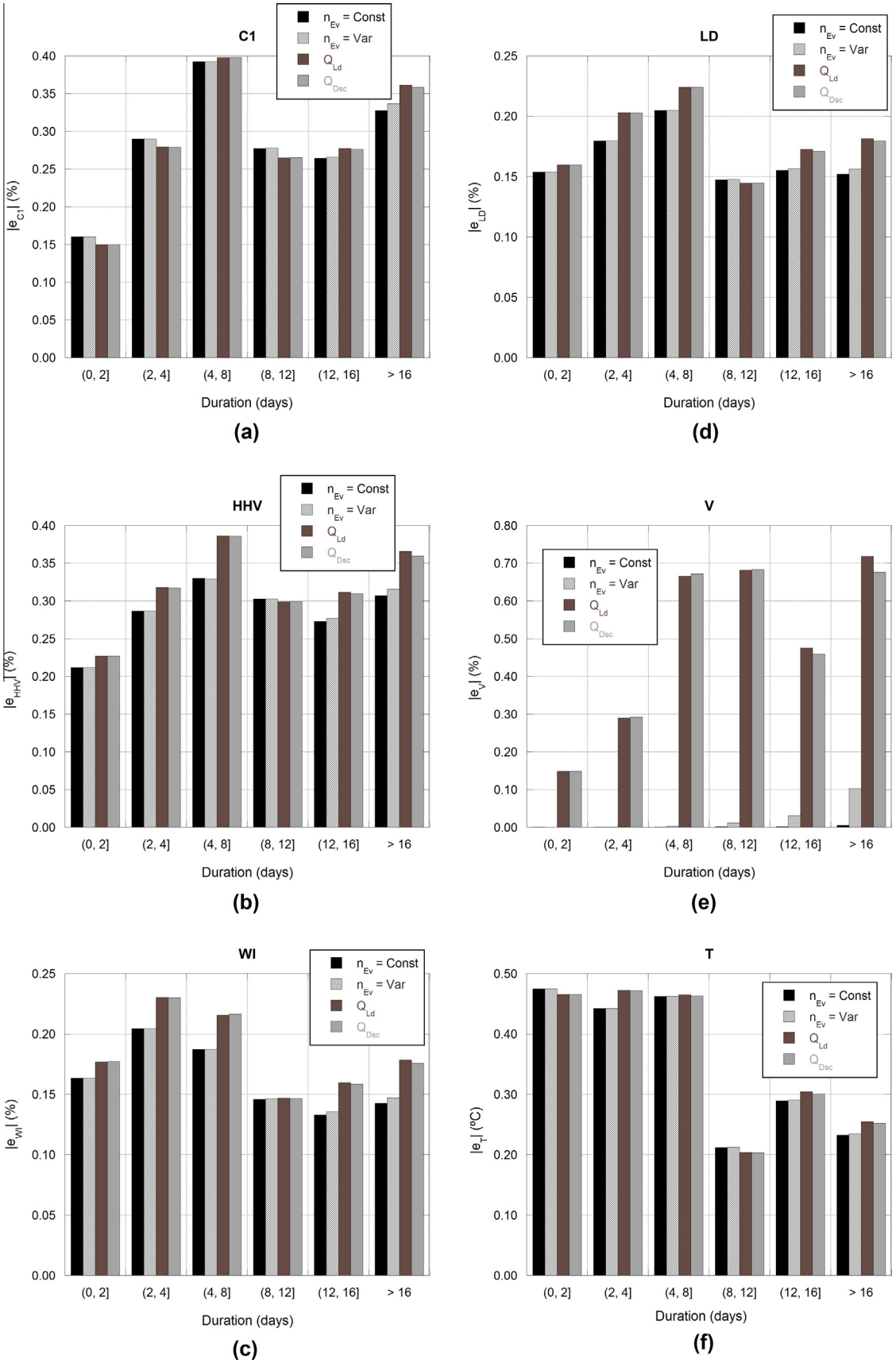

Fig. 5. Average relative errors for the different ageing models: influence of voyage duration for C1 (a), HHV (b), WI (c), LD (d), volume (e) and temperature (f).

Table 4
Classification of voyages into duration and ship capacity.

		Ship capacity					
		SNGC (0, 60,000]	HNGC (60,000, 125,000]	MNGC (125,000, 150,000]	LNGC (150,000, 177,000]	VLNGC > 177,000	Total
Voyage duration	Immediate voyages (0, 2] days	31	12	6	0	0	49
	Very short voyages (2, 4] days	49	25	6	0	0	80
	Short voyages (4, 8] days	32	2	26	4	0	64
	Medium voyages (8, 12] days	3	6	142	7	0	158
	Large voyages (12, 16] days	2	28	133	2	2	167
	Very large voyages >16 days	0	8	31	1	0	40
Total		117	81	344	14	2	558
Number of ships		3	7	58	8	2	

The heat flow ageing approach comprises two different models, considering that the vapour enthalpy of the vented mols is calculated under loading or unloading conditions. The real vented enthalpy lies between these two limiting values, hence they represent the upper and lower boundaries for this parameter.

2.5. Validation

The four different ageing models are first tested against published references. The numerical and experimental data available in [6,7] were already used for validation in [15], so they are not repeated here due to the minor differences with those initial ageing models. The experimental data available in [4] cannot be reproduced with the current ageing models since the evaporation rate is unknown and there is a significant diminishing of both liquid and vapour flows (up to 15%) that greatly alters the formulation of the current ageing models.

Table 2 displays the available numerical data obtained from Shah and Aarts [5] and the results obtained using the different proposed ageing models. The comparison is based on the difference between published data and current numerical results obtained by through the aforementioned ageing models:

$$e_i = \frac{\phi_{Ref} - \phi_i}{\phi_{Ref}} \cdot 100 \tag{31}$$

where subscript i referrers to ageing model i. Only three ageing models are tested in this exercise: constant evaporation rate (Eq. (16)), variable evaporation rate (Eq. (30)) and constant heat flow. Since the final composition and temperature is not available in [5], it is impossible to estimate a priori the energy content of the tank at the end of the ageing period. Hence, only the imposed heat flow defined in [5] is applied.

Shah and Aarts report results for 9 different ageing cases in [5]. Cases 1 to 8 are devoted to a flat bottomed LNG storage tank, while Case 9 simulates the weathering during ship transportation. Table 2 displays the available data for these cases and it is assumed that the tank is fully loaded in all cases. Cases 1 and 2 evaluate the influence of the heat flow received by a 300,000 bbl (~47,691 m^3) tank over 270 days. For Case 1, the best match in terms of the temperature and Higher Heating Value (HHV) is achieved by of constant heat flow model, as would be expected given the numerical model defined in [5] is also based on this approach. HHV is calculated from GPA 2172 norm [31], considering combustion and metering conditions of 15 °C and 1 bar (60 °F and 14.696 psia). For Case 2, the differences are significantly greater for all ageing models. However, it should be noted that the received heat flow in Case 2 is double that in Case 1, while BOR remains unchanged. Cases 3 to 5 are not reported here because the N2 content in the LNG mixture is 15%, 10% and 5%, respectively, and the available thermodynamic functions defined in Table 1 can handle a maximum N2 content of only 4% [30]. Cases 6 to 8 evaluate the influence of LNG composition on HHV, revealing that the best adjustment is achieved by the variable evaporation rate ageing model. Case 6 shows no ageing effects, as the LNG comprises only Methane. For Case 9, the lowest difference is achieved for HHV and Liquid Density (LD) by the constant heat flow ageing model, while the best temperature match comes from the variable evaporation rate ageing model.

Then, the defined ageing models are tested against the numerical results reported by Dimopoulos and Frangopoulos [12], which reports on the ageing of an LNG mixture over a 25-day ship transportation. A heat flow of 600 kW is imposed and the integration of the plot of BOR against time yields an average value of 0.1382%/day. The ship capacity is 150,000 m^3 and it is assumed that the LNG fully occupies this volume. No pressure data is reported, so it is assumed that the LNG is at atmospheric pressure. The initial LNG temperature is −163 °C and a temperature rate of change defined by a constant of 0.5 K/day is specified, although this parameter would yield a temperature of −150.5 °C by the end of the voyage. If an iterative loop is performed by changing the LNG temperature at the discharge port to calculate the corresponding heat flow using Eq. (24), an LNG temperature of −159.784 °C is obtained at the discharge port which would yield a heat flow of 600.169 kW. For validation purposes, the differences in the molar compositions of both liquid (X) and vapour (Y) phases at the end of the voyage are compared in Table 3. The best match is achieved by the constant evaporation rate model. It must be noted that the composition of the vapour phase at the initial step is also provided in [12]. The comparison with the obtained values by the current ageing models reveals large differences, especially for N2. This is caused by the different vapour–liquid equilibrium calculation models. The validity of the current ageing models based on Lee–Erbar–Edmister equation of state can be checked by comparing the corresponding vapour compositions with those obtained by the GERG2004 equation of state [32,33]. Both equations of state yield nearly the same differences with respect to the published BOG composition at loading conditions, so it is clear that thermodynamic functions play a key role in the accuracy of ageing phenomena.

In any case, since the difference between the current ageing models and the other numerical models described in the literature is less than 1% for the main variables including C1, HHV or LD in most cases, the validity of the proposed ageing models can be ensured.

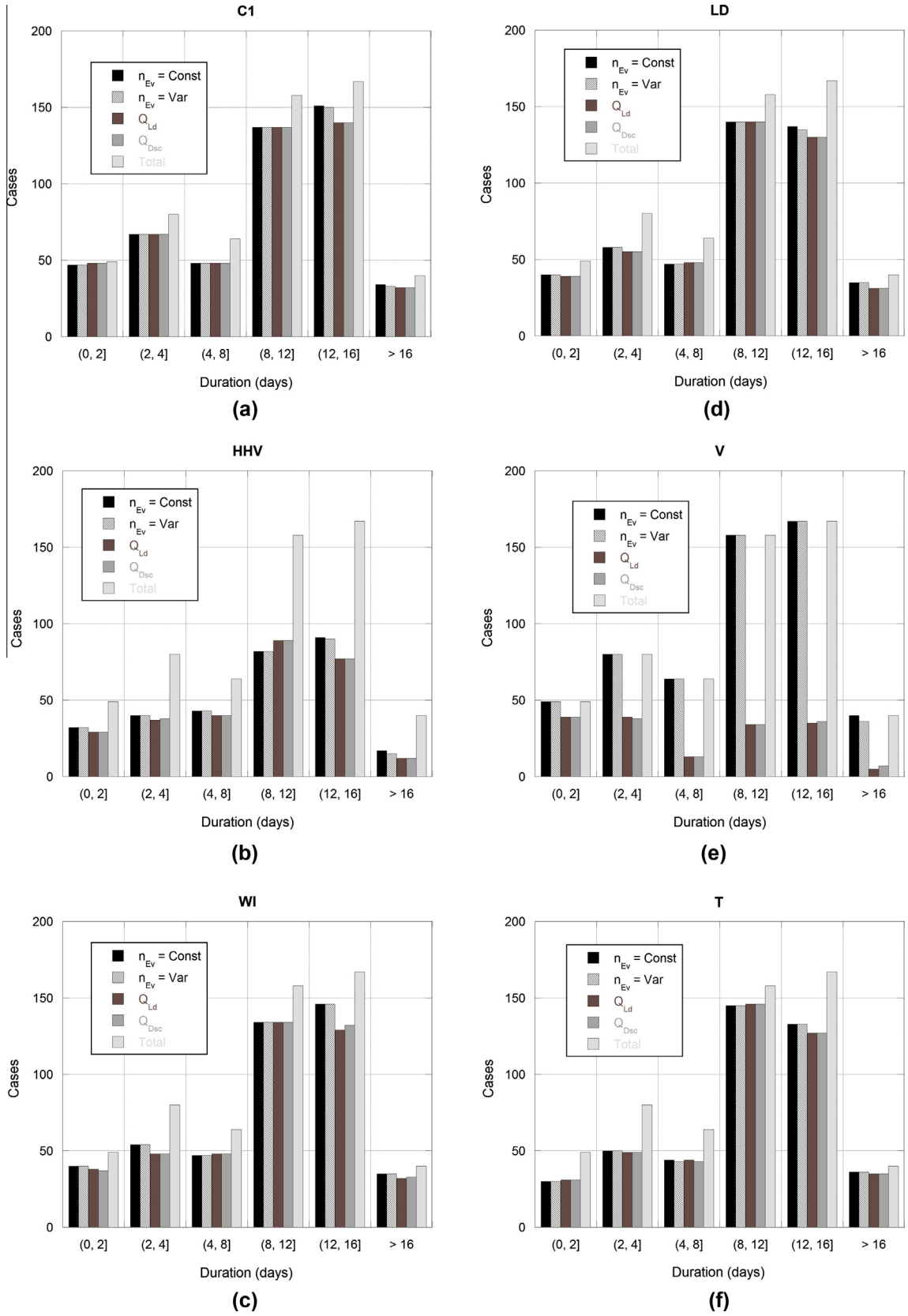

Fig. 6. Number of cases which meet the limiting errors: influence of voyage duration for C1 (a), HHV (b), WI (c), LD (d), volume (e) and temperature (f).

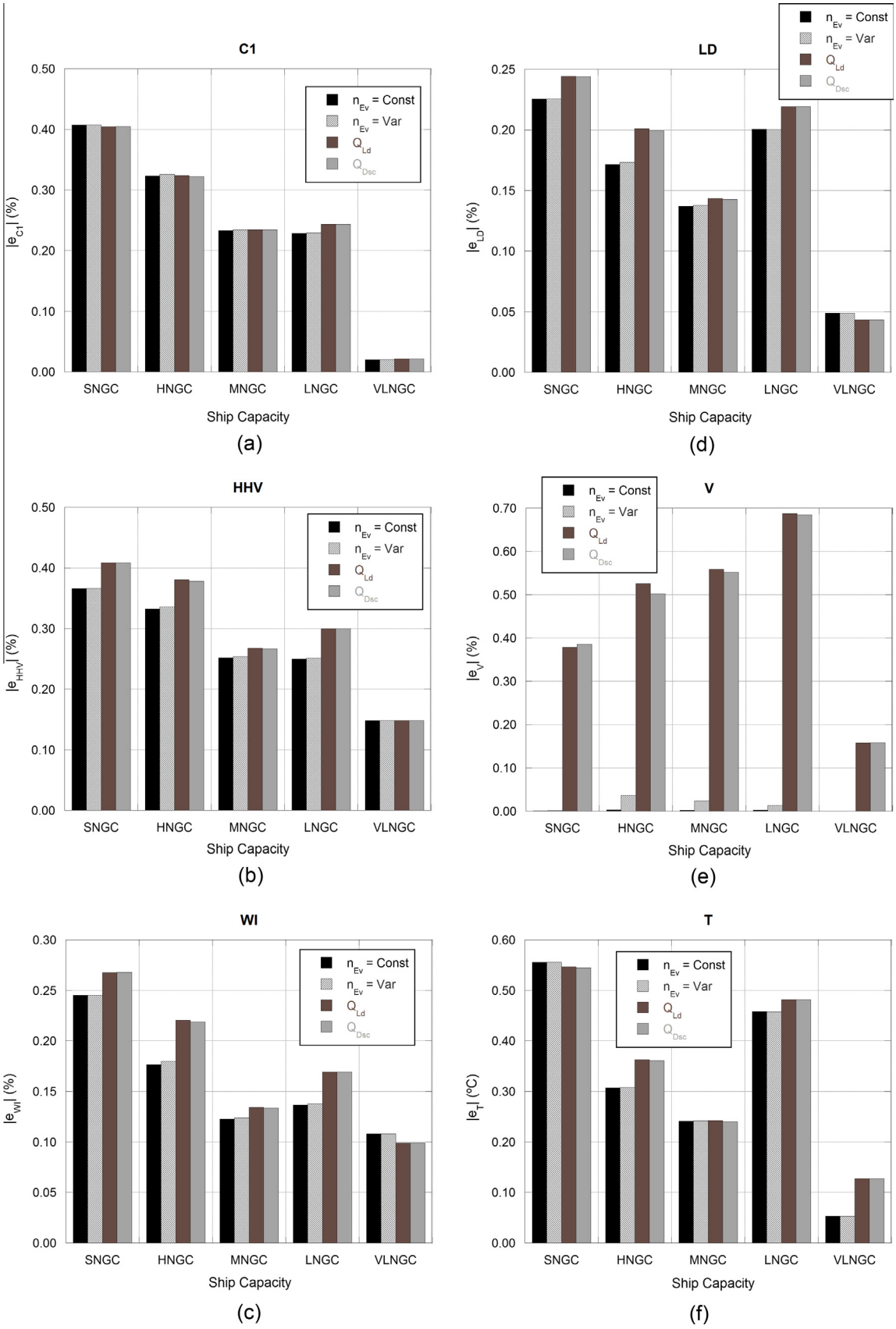

Fig. 7. Average relative errors for the different ageing models: influence of ship capacity for C1 (a), HHV (b), WI (c), LD (d), volume (e) and temperature (f).

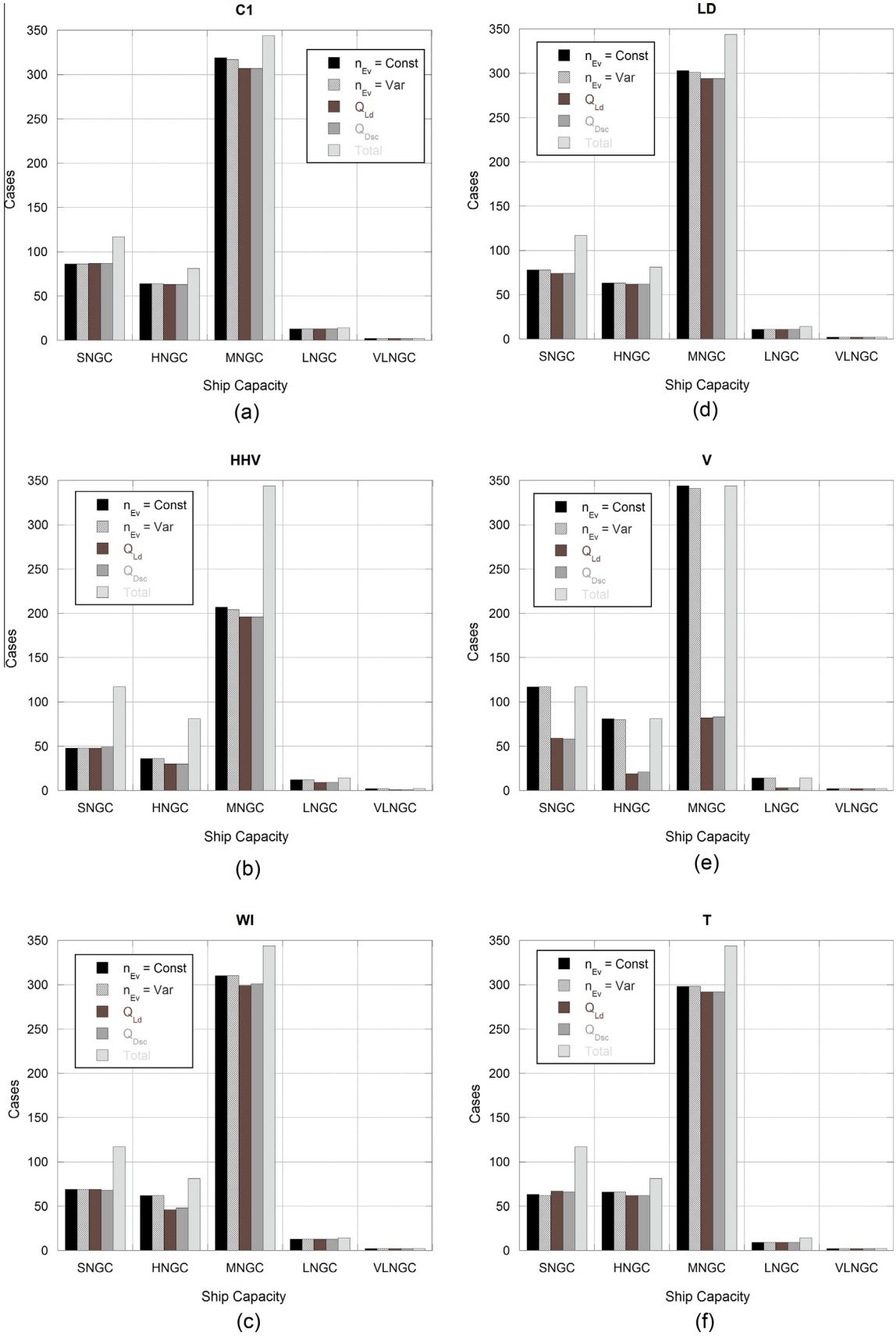

Fig. 8. Number of cases which meet the limiting errors: influence of the ship capacity for C1 (a), HHV (b), WI (c), LD (d), volume (e) and temperature (f).

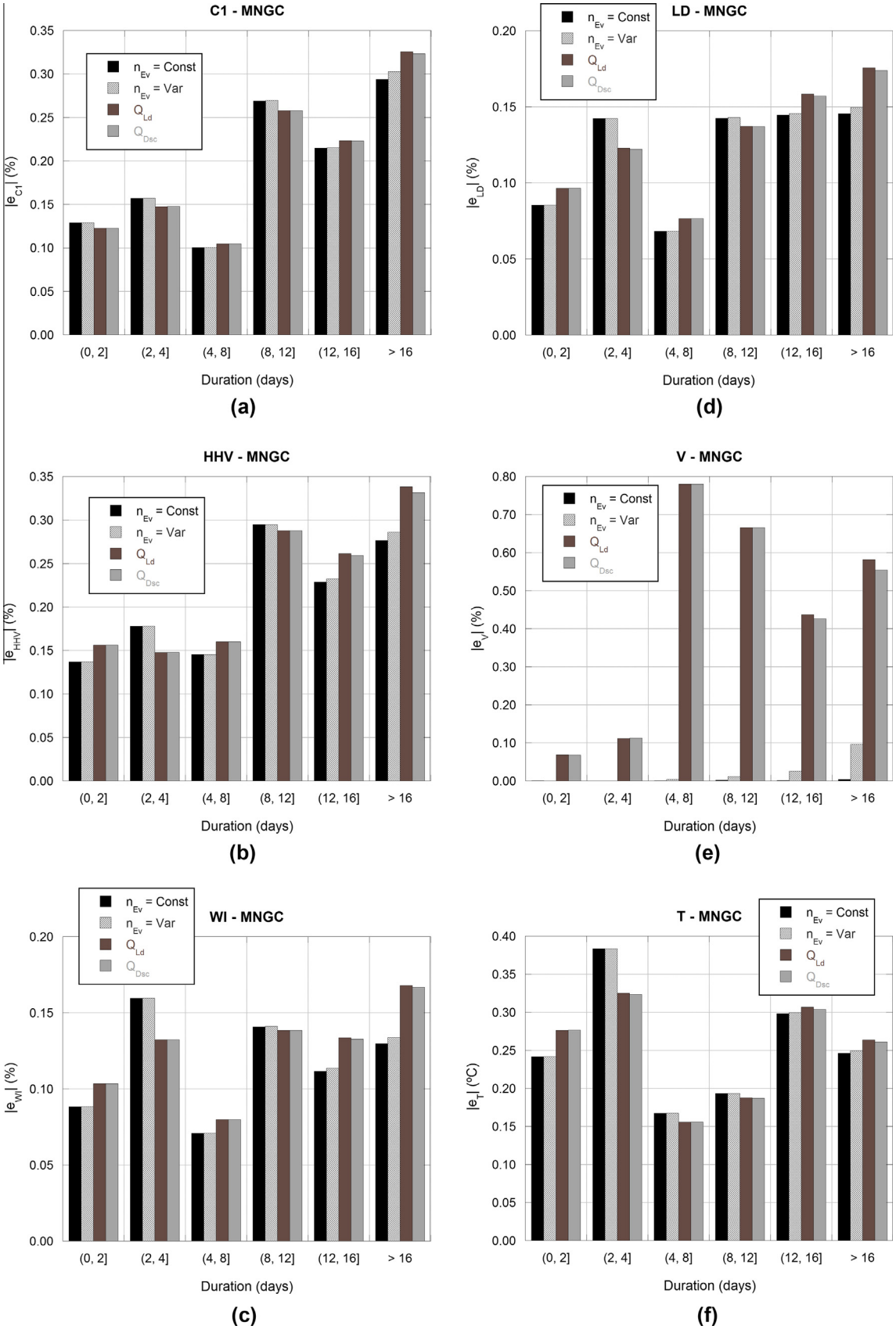

Fig. 9. Average relative errors for the different ageing models: influence of voyage duration on MNCG ships for C1 (a), HHV (b), WI (c), LD (d), volume (e) and temperature (f).

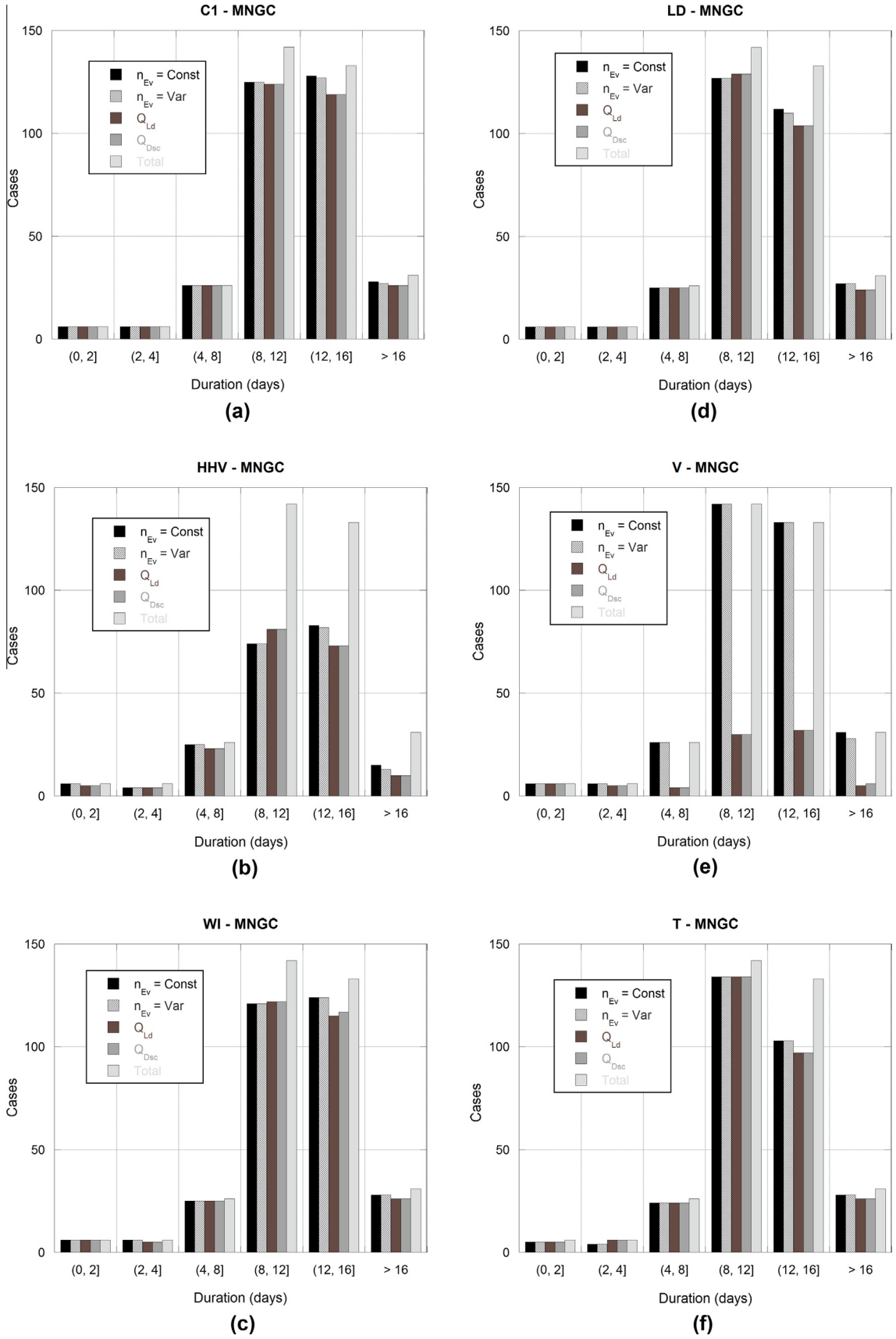

Fig. 10. Number of cases which meet the limiting errors: influence of voyage duration on MNCG ships for C1 (a), HHV (b), WI (c), LD (d), volume (e) and temperature (f).

3. Results

3.1. Global analysis for the full database

A direct consequence of the current analysis is the application of the best model for ageing predictions to real shipping data. It is desirable that a minimum amount of data should be defined by the user, but it must be accurate enough to predict LNG ageing in a large number of situations. The available data collected for this study comprises 558 voyages lasting from 17.5 h to 1655 h, with an initial Methane content ranging from 80.57% to 98.11%, and 78 different ships of a capacity varying from 29,600 m^3 to 216,200 m^3. Thus, a comparison of the results obtained from the previously defined models with the limited set of data available in the literature cannot provide the best answer to the wide spectrum of LNG ageing phenomena during ship transportation given the uncertainties described in Section 1.

The accuracy of the proposed ageing models is checked for the following selected variables at the discharge port: molar fraction of C1, HHV, WI and LD. The relative difference, also defined through Eq. (31), is limited for each variable to the following maximum values: ±0.5% for C1, ±0.25% for HHV and WI and ±0.27% for LD [34]. These limits represent the maximum allowable differences in measurement procedures for LNG composition and properties. Hence, if the differences between measured values in regasification plants and the results predicted by each ageing model are lower than these limits, the numerical estimation is within the admitted uncertainty of the measurement itself. Additionally, the predicted LNG volume and the temperature at the discharge port are compared with experimental data, allowing a maximum relative difference of ±0.21% for volume and a difference of ±0.5 °C for temperature [3].

Fig. 3a compares the average of the relative errors for all cases contained in the database. In general, it can be concluded that all ageing models are quite similar and no single model stands above the rest. It is clear that the best match for the prediction of discharged LNG volume is achieved through the constant evaporation rate model, but the approximation at constant heat flow when the vented enthalpy is calculated under discharged conditions shows the lowest differences for all other variables, i.e. C1, HHV, WI, LD and temperature. On the contrary, in Fig. 3b, the number of cases which match the proposed limiting criteria shows a significant difference between the ageing evaporation rate and heat flow models: the prediction of the discharged volume is significantly worse for both approaches at a constant heat flow. The constant heat flow models predict a lower evaporation rate, though the final temperature is more accurately captured using these approximations.

Fig. 4 shows the percentage of cases inside the error limits for the six analysed variables. It is again demonstrated that all the proposed ageing models are similar accurate but for the case of the constant evaporation rate for the volume prediction, which is undoubtedly the best option for this variable. The Methane content and Liquid Density tend to be overpredicted by the ageing models because most of the relative errors are negative.

3.2. Analysis of voyage duration and ship capacity

The suitability of the proposed ageing models is next checked against two independent variables: the voyage duration and the ship capacity. As stated in Section 2.1, the ageing models are based on the assumption of thermodynamic equilibrium between the liquid and vapour phases. Thus, if the voyage is too short, it could be difficult to achieve the thermodynamic equilibrium. Likewise, small ships are usually old ships, receiving a larger proportional heat flow than newer well insulated ships. Lastly, small ships tend to receive larger heat flows than bigger ones, since ratio volume/heat transfer area ratio grows as the ship volume increases.

The length of the voyage is organized into 6 blocks of 2 or 4 days: immediate voyages are considered those lasting less than 2 days. Very short voyages are considered to be between 2 and 4 days, while short voyages last for 4–8 days. Medium voyages are defined as those between 8 and 12 days while large voyages are considered to be between 12 and 16 days. Finally, very long voyages last over 16 days.

References [1,35] provide several segments to classify ships according to their capacity. Based on these, the current investigation organizes ship capacity into five segments: the smallest ships are divided into two classes: SNGC (Small Natural Gas Carriers), having a capacity up to 60,000 m^3 and HNGC (Handy Natural Gas Carriers), ranging from 60,000 m^3 to 125,000 m^3. MNGC (Medium Natural Gas Carriers) are those between 125,000 m^3 and 150,000 m^3 while LNGC (Large Natural Gas Carriers) are those between 150,000 m^3 and 177,000 m^3. Lastly, VLNGC (Very Large Natural Gas Carriers) are defined as LNG tankers with a capacity greater than 177,000 m^3.

Given the above classification, Table 4 displays the number of voyages in each category and the number of different ships in the current database. The database does not show a regular distribution among the 30 different categories: MNGC for medium and lengthy voyages represents nearly half of the voyages in the database. Then, an initial analysis is presented first in terms of the ship capacity and the voyage duration and afterwards, the influence of the two variables is checked for the most representative ship capacity in the database and in the LNG fleet: the MNGC category [1].

Figs. 5 and 6 show the average relative errors defined by Eq. (31) and the number of cases which meet the imposed limits for the different ageing models and for the different voyage durations. For a more comprehensive comparison, average errors displayed in the following figures are calculated to an absolute value, to avoid values on opposite sides nullifying each other. C1 is underpredicted for immediate to short voyages, but after 8 days, the calculated Methane content in the LNG mixture is overpredicted. For HHV, WI and LD, the voyage duration has a lower influence on the average error. However, for the temperature, the best predictions are those for long voyages, as could be expected. The ageing models are based on instant equilibrium conditions, so the trans-

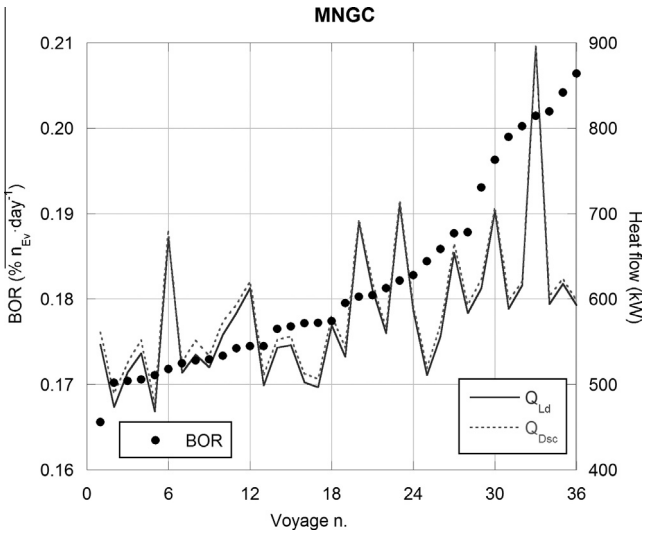

Fig. 11. Comparison of BOR and heat flow for a single MNGC ship.

formation from loading conditions to initial equilibrium conditions is not as instantaneous as proposed. Further research should be undertaken on this point. Meanwhile, worse predictions for volume are obtained when voyage duration is increased, especially in the ageing models based on heat flow. The numbers of cases that meet the limiting errors are significantly reduced for HHV and voyages lasting from 8 to 16 days. A similar conclusion can be drawn from Figs. 7 and 8 regarding ship capacity. The average error decreases as the ship capacity increases. LNGC shows certain discrepancies with this tendency, probably due to the difficulties in achieving a good statistical description for this category, since there have only been 14 voyages by 8 different ships.

Figs. 9 and 10 report the influence of duration on the relative error and the number of cases which meet the limiting criteria for the MNGC ships alone. As a consequence, there are no significant differences between the behaviour observed in the full

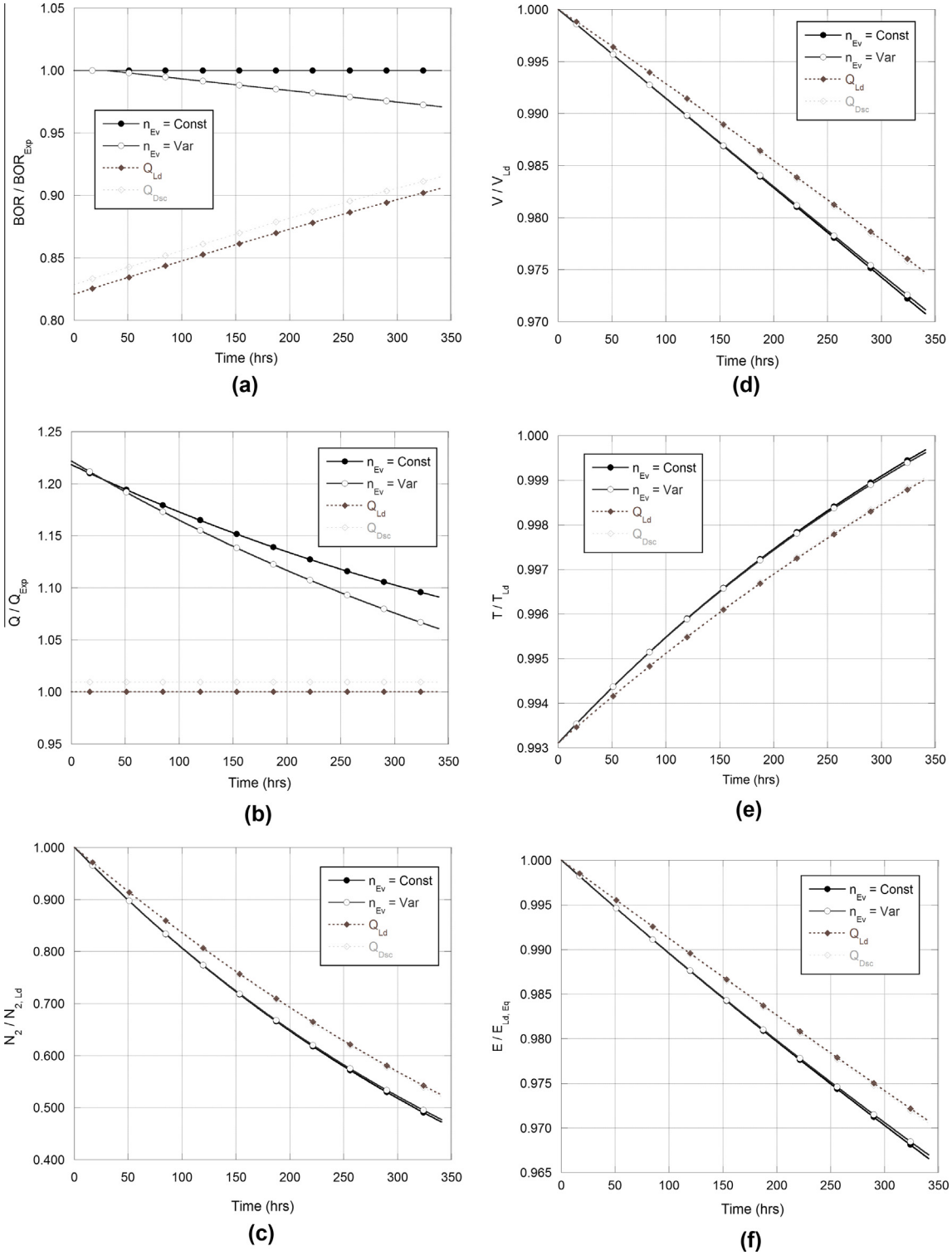

Fig. 12. Evolution over time of BOR (a), heat flow (b), N2 content (c), LNG volume (d), temperature (e) and energy content (f) for one voyage of a single MNGC ship.

database and in the results obtained for this type of ship; for example, it should be noted that HHV, WI, LD and temperature show a certain drop in the average relative error for voyages lasting from 4 to 8 days when only MNGC ships are considered.

3.3. Detailed analysis for a single ship and a single voyage

The BOR and heat flow for a single ship are compared in Fig. 11. The selected ship is a Moss-type MNGC ship with a capacity of 126,300 m^3. It was built 40 years ago and is propelled by a dual fuel engine that can burn LNG. There are 36 reported trips in the current database. These voyages have the same origin, with variations of less than 1% in the initial C1 content and temperature. The voyage varies from 13 to 23 days. Per the available data, the BOR varies from 0.1656% to 0.2064%, meaning a relative variation of 19.76% between these extreme values. However, the heat flow obtained through Eq. (24) can be expanded from 468 kW to 895 kW (when the enthalpy of the vented flow is calculated at the loading conditions), and this represents a difference of 47.73%.

Fig. 12 describes in detail the voyage of the aforementioned ship with the largest BOR. The measured values at the loading and discharge ports are collected in Table 5. The trip lasted for 341 h. The comparison of BOR in Fig. 12a shows that evaporation is more vigorous for ageing models defined by the evaporation rate. The difference between the constant and variable evaporation rates is not significant, about 2.90% at the end of the voyage, compared to the difference with the BOR obtained through constant heat flow models, which is in the range of 10–18% lower than the BOR constant. This is also seen in Fig. 12b, where the heat flow obtained by ageing models defined according to evaporation rate is about 20% greater than the heat flow calculated using Eq. (24). The change in nitrogen content over time is shown in Fig. 12c to describe the variations in the most volatile compound. Once more, the more vigorous evaporation from BOR ageing models is revealed, yielding the greatest accuracy, considering that the quotient of N2 content experimentally measured is 0.4205 at the end of the voyage. The liquid volume quotients in Fig. 12d follow the same pattern, i.e. the evaporation rate ageing models are closer to the experimental value of 0.9707 than the heat flow ageing models.

Lastly, the superheated state of loaded LNG is proven in Fig. 12e. The temperature at the beginning of the voyage is 0.7% less than the loading temperature. This means that the LNG must be cooled somehow after loading. This initial cooling step is not simulated by the current ageing models; the LNG is simply considered to be at the new equilibrium conditions so further investigations should examine this feature to improve the accuracy of the current ageing approaches to model this initial transformation. Fig. 12f plots the evolution over time of the energy content carried by the ship. In this image, the energy content is compared with the equilibrium conditions at the loading point to facilitate easier its interpretation. Over time, the energy content of the tank is reduced by up 3.3% for evaporation rate models and 2.9% for heat flow models.

Table 5
Measured values at loading and discharge ports for the case of maximum BOR.

Variable	Loading	Discharge
C1 (%)	90.438	90.103
C2 (%)	6.000	6.422
C3 (%)	2.240	2.300
iC4 (%)	0.370	0.394
*n*C4 (%)	0.550	0.603
iC5 (%)	0.010	0.012
*n*C5 (%)	0.002	0.01
N2 (%)	0.390	0.164
P (mbar)	1129	1129
T (°C)	−159.60	−159.25
T_{Eq} (°C)	−160.38	−159.53
V (m^3)	111944.2	108660.73
HHV (MJ/m^3)	157.608	158.796
WI (MJ/m^3)	199.908	200.952
LD (kg/m^3)	456.244	457.137
n_L (kmol)	2844838.95	2753460.30
n_V (kmol)	1789.60	2192.91
Q_{Exp} (kW)	592.39	598.04

4. Conclusions and further work

The comparison between the different ageing models reveals that, in general, the approaches defined by the evaporation rate show a better prediction than those of constant heat flow. As expected, the ageing model based on constant evaporation rate yields the best approach for the LNG volume at the discharge port. For the other variables, there are no significant differences between the ageing models based on constant or variable evaporation rates. On the contrary, the ageing models based on constant heat flow, calculated at the loading or the discharge ports, achieve greater errors than the other approach.

Increasing the length of the voyage and/or the ship capacity reduces the average errors among the ageing models. This is probably caused by the generally assumed hypothesis of thermodynamic equilibrium between liquid and vapour phase, which is more plausible for longer voyages and greater ship capacities.

There are significant uncertainties described in the literature that prevent a simple modelling of LNG ageing during ship transportation based on the heat flow transferred from the environment alone. Hence, the definition of a global parameter like BOR can provide a more accurate answer to the prediction of the full weathering phenomena. However, how can BOR be anticipated when no data is available at the discharge port?

At the present, there is no definitive answer to this question. There are some guides to selecting typical BOR values, but, as demonstrated in Section 3, the same ship on the same route can show variations in BOR of 20%. As a consequence, a considerable effort should be made to achieve a better modelling of the ageing phenomena. Acquiring more detailed experimental results is necessary to define and test new ageing approaches. For example, the data below should be provided in this context:

- accurate data for tank pressure over time;
- measurement or calculation of the overall heat transfer coefficient from the environment to the LNG considering real thermal properties of insulation materials, ship velocities and sea and air temperatures;
- on-boards measurements of temperature and composition during ship transportation, together with accurate definitions of the initial and final heel compositions;
- in depth knowledge about ship filling and empting processes, and determination of BOR generated during these;
- full description of BOR handling during ship transportation;
- reliable thermodynamic data for non equilibrium conditions.

In the meantime, the current ageing approaches described in this paper can provide an initial estimation of ageing data during ship transportation.

Acknowledgement

This diffusion work has been partly funded by the FEDER Operative Programme for Aragon (2007–2013).

References

[1] International Gas Union. World LNG report – 2015 edition. C/ O Statoil ASA, Norway: International Gas Union, Office of the Secretary General. Available

online at <http://www.igu.org/sites/default/files/node-page-field_file/IGU-World%20LNG%20Report-2015%20Edition.pdf> [last access: September, 28th, 2015].
[2] BP. BP energy outlook 2035. Available online at <http://www.bp.com/content/dam/bp/pdf/Energy-economics/energy-outlook-2015/Energy_Outlook_2035_booklet.pdf> [last access: September, 28th, 2015].
[3] GIIGNL. Custody transfer handbook. Lallois (France): International Group of Liquefied Natural Gas Importers; 2011.
[4] Acker GH, Moulton DS. LNG weathering effects – theoretical and empirical. Topical report No. GRI – 9210464. Gas Research Institute; 1992.
[5] Shah JM, Aarts JJ. Effect of weathering of LNG in storage tanks, advances in cryogenic engineering. New York: Springer; 1995.
[6] Kountz KJ. Weathering of on-board storage tanks. Project final report. IGT project 32034 – 02. Institute of Gas Technology; 1999.
[7] Aspelund A, Gjøvåg GA, Nekså P, Kolsaker K. LNG – chain, a calculation tool for natural gas quality in small scale lng distribution chains. CR06 – 133, ICEC – 21, Prague; 2007.
[8] Boe R. Pool boiling of hydrocarbon mixtures on water. Int J Heat Mass Transf 1998;41:1003–11.
[9] Conrado C, Vesovic V. The influence of chemical composition on vaporization of LNG and LPG on unconfined water surfaces. Chem Eng Sci 2000;55:4549–62.
[10] Bates S, Morrison DS. Modeling the behaviour of stratified liquid natural gas in storage tanks: a study of the rollover phenomenon. Int J Heat Mass Transf 1997;40:1875–84.
[11] Chen QS, Wegrzyn J, Prasad V. Analysis of temperature and pressure changes in liquefied natural gas (LNG) cryogenic tanks. Cryogenics 2004;44:701–9.
[12] Dimopoulos GG, Frangopoulos CA. A dynamic model for liquefied natural gas evaporation during marine transportation. Int J Thermodyn 2008;11:123–31.
[13] Pellegrini LA, Moioli S, Brignoli F, Bellini C. LNG technology: the weathering in above-ground storage tanks. Ind Eng Chem Res 2014;53:3931–7.
[14] Migliore C, Tubilleja C, Vesovic V. Weathering prediction model for stored liquefied natural gas (LNG). J Nat Gas Sci Eng 2015;26:570–80.
[15] Miana M, del Hoyo R, Rodrigálvarez V, Valdés JR, Llorens R. Calculation models of liquefied natural gas (LNG) ageing during ship transportation. Appl Energy 2010;87:1687–700.
[16] Dobrota D, Lalić B, Komar I. Problem of Boil-off in LNG supply chain. Trans Maritime Sci 2013;2:91–100.
[17] Kim YM, Ko SC, Chun BI, Kim KK. A study on the thermal design of the cryogenic LNG carrier. J Korean Soc Mar Eng 1993;17:1–10.
[18] Kim JG, Kim YM, Kim CS. A study on unsteady temperature distribution analysis of moss type LNG carrier by insulation system. J Ocean Eng Technol 1997;11:159–68.
[19] Heo JH, Lee YB. Heat flux calculation for thermal equilibrium of cofferdam in a LNG carrier. J Soc Naval Arch Korea 1998;35:98–106.
[20] Song SO, Lee JH, Jun HP, Sung BY, Kim KK, Kim SG. A study on the three-dimensional steady state temperature distribution and BOR calculation program development for the membrane type LNG carrier. J Korean Soc Mar Eng 1999;23(2):140–9.
[21] Miana M, Legorburo R, Diez D, Hwang YH. Calculation of boil-off rate of liquefied natural gas in mark III tanks of ship carriers by numerical analysis. Appl Therm Eng 2016;93:279–96.
[22] Sonnenschein M, Wendt BL, Schrock AK, Sonney JM, Ryan AJ. The relationship between polyurethane foam microstructure and foam aging. Polymer 2008;49:934–42.
[23] Lattuati-Derieux A, Thao-Heu S, Lavédrine B. Assessment of the degradation of polyurethane foams after artificial and natural ageing by using pyrolysis-gas chromatography/mass spectrometry and headspace-solid phase microextraction-gas chromatography/mass spectrometry. J Chromatogr A 2011;1218:4498–508.
[24] Neill DT, Hashemi HT, Sliepcevich CM. Boil-off rates and wall temperatures in aboveground LNG storage tanks. Adv Cryogenic Heat Transf, Chem Eng Prog Symp Ser 1968(87):111–9.
[25] Huang S, Hartono J, Pankaj S. BOG recovery from long jetties during LNG ship-loading. In: 15th International conference & exhibition on liquefied natural gas, Barcelona; 2007.
[26] Andrianos K. Techno-economic evaluation of various energy systems for LNG carriers. Diploma thesis. Athens, Greece: National Technical University of Athens; 2006.
[27] Lee BL, Erbar JH, Edmister WC. Liquefied natural gas: thermodynamic properties at low temperatures. Chem Eng Prog 1972;68:83–4. 99.
[28] Lee BL, Erbar JH, Edmister WC. Prediction of thermodynamic properties for low temperature hydrocarbon process calculations. AIChE J 1973;19:349–53.
[29] Rijkers MPW, Heidemann RA. Convergence behaviour of single-stage flash calculations. ACS Symp Ser 1986;300:476–93.
[30] McCarty RD. Four mathematical models for the prediction of LNG densities. NBS technical note 1030. Boulder (USA); 1980.
[31] Gas Processors Association. GPA Standard 2172-96. Calculation of gross heating value, relative density and compressibility factor for natural gas mixtures from compositional analysis; 2009.
[32] Wagner W. Description of the general software package for the calculation of the thermodynamic properties from the GERG–2004 wide-range reference equation of state for natural gas. Ruhr: Universität Bochum; June 2005.
[33] Kunz O, Klimeck R, Wagner W, Jaeschke M. The GERG-2004 wide-range equation of state for natural gases and other mixtures. GERG technical monograph TM 15 2007. Düsseldorf; 2007.
[34] ENAGAS. Especificación técnica EV 203 de sistemas analíticos para análisis en continuo y discontinuo de gas natural para facturación. Revisión 4, Madrid (Spain); 2009.
[35] Danmarks Skibskredit A-S (Danish Ship Finance) – Segments. Available online at <http://www.shipfinance.dk/en/SHIPPING-RESEARCH/Tankskibe/LNG-Tankskibe/Segmenter> [last access: September, 28th, 2015].